



The multi-year contribution of Indo-China peninsula fire emissions to aerosol radiation forcing in southern China during 2013–2019

Jun Zhu^a, Xu Yue^{a,*}, Hao Zhou^b, Huizheng Che^c, Xiangao Xia^{d,e}, Jun Wang^f, Tianliang Zhao^g, Chenguang Tian^a, Hong Liao^a

^a Jiangsu Key Laboratory of Atmospheric Environment Monitoring and Pollution Control, Collaborative Innovation Center of Atmospheric Environment and Equipment Technology, School of Environmental Science and Engineering, Nanjing University of Information Science & Technology (NUIST), Nanjing, 210044, China

^b College of Meteorology and Oceanography, National University of Defense Technology, Changsha, 410073, China

^c State Key Laboratory of Severe Weather (LASW) and Key Laboratory of Atmospheric Chemistry (LAC), Chinese Academy of Meteorological Sciences, CMA, Beijing, 100081, China

^d LAGEO, Institute of Atmospheric Physics, Chinese Academy of Sciences, Beijing 100029, China

^e University of Chinese Academy of Sciences, Beijing, 101408, China

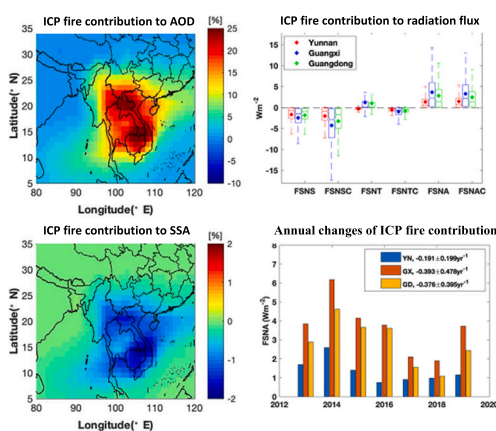
^f Center of Global and Regional Environmental Research and Department of Chemical and Biochemical Engineering, University of Iowa, Iowa City, Iowa, USA

^g Key Laboratory for Aerosol-Cloud-Precipitation of China Meteorological Administration, Nanjing University of Information Science and Technology, Nanjing 210044, China

HIGHLIGHTS

- Multi-year contributions of fire transport to ARF in southern China were quantified.
- ICP fire increase AOD 0.1 (15 %) and reduce SSA in three Chinese regions in 2013–2019.
- Fire contributed -5 Wm^{-2} to the annual ARF and about -15 Wm^{-2} in the daily case.
- The general trends of smoke impact in southern China declined during 2013–2019.

GRAPHICAL ABSTRACT



ARTICLE INFO

Editor: Jianmin Chen

Keywords:
Smoke aerosol
Aerosol radiation forcing
Southeast Asia

ABSTRACT

Fire emissions in Southeast Asia transported to southern China every spring (March–May), influencing not only the air quality but also the weather and climate. However, the multi-year variations and magnitude of this impact on aerosol radiation forcing in southern China remain unclear. Here, we quantified the multi-year contributions of fire emissions in Indo-China Peninsula (ICP) region to aerosol radiation forcing in the various southern Chinese provinces during the fire season (March–May) of 2013–2019 combining the 3-dimension chemical transport model and the Column Radiation Model (CRM) simulations. The models' evaluations showed they reasonably

* Corresponding author.

E-mail address: yuxu@nuist.edu.cn (X. Yue).

<https://doi.org/10.1016/j.scitotenv.2024.172337>

Received 19 December 2023; Received in revised form 6 April 2024; Accepted 7 April 2024

Available online 10 April 2024

0048-9697/© 2024 Elsevier B.V. All rights reserved.

capture the temporal and spatial distribution of surface aerosol concentrations and column aerosol optical properties over the study regions. The fire emissions over the ICP region were found to increase the aerosol optical depth (AOD) value by 0.1 (15 %) and reduce the single scattering albedo (SSA) in three southern regions of China (Yunnan-YN, Guangxi-GX, and Guangdong-GD from west to east), owing to increases in the proportions of black carbon (BC, $0.4 \% \pm 0.1 \%$) and organic carbon (OC, $3.0 \% \pm 0.9 \%$) within the aerosol compositions. The transported smoke aerosols cooled surface but heated the atmosphere in the southern China regions, with the largest mean reduction of -5 Wm^{-2} (-3%) in surface shortwave radiation forcing and the maximum daily contributions of about -15 Wm^{-2} (-15%) to the atmosphere radiation forcing in the GX region, followed by the GD and YN regions. The impacts of ICP fire emissions on aerosol optical and radiative parameters declined during 2013–2019, with the highest rate of $0.393 \pm 0.478 \text{ Wm}^{-2} \text{ yr}^{-1}$ in the GX for the shortwave radiation forcing in the atmosphere. Besides, their yearly changes in the contribution were consistent with the annual fire emissions in the ICP region. Such strong radiative perturbations of ICP fire emissions were expected to influence regional meteorology in southern China and should be considered in the climate simulations.

1. Introduction

Fire emission is an important source of various trace gases and aerosols, affecting not only the air quality but also the regional weather and climate in both the source and downwind areas (Ajoku et al., 2021; Che et al., 2024; Li et al., 2016; N.-H. Lin et al., 2014; Liu et al., 2020; Zhu et al., 2014). The robust predictive tools, such as Artificial Intelligence (AI) and advanced machine learning-based models, are established for evaluating and forecasting the fire events and their impacts in recent years (Donnelly et al., 2024; Yeganeh-Bakhtiary et al., 2022). While observations and models' simulations are widely used to assess of these fire impacts (Chuvienco et al., 2008; Ford et al., 2018; Hantson et al., 2016).

The impact of smoke transport has been well studied at the global scale (Tian et al., 2023; Tosca et al., 2013) and in regions with frequent fire activities, such as Central America (Saide et al., 2015; Wang and Christopher, 2006), Russia (Li et al., 2019; Mielonen et al., 2012; Péré et al., 2014) and Africa (Ansmann et al., 2009; Williams et al., 2012). South and Southeast Asia also exist frequent fire activities in fire seasons, as the Indo-China Peninsula (including Myanmar, Thailand, Laos, Vietnam, and Cambodia, hereafter referred to as the ICP), there are frequent fire activities every spring (March–May) due to slash-and-burn and land-clearing practices (Fox et al., 2009; Jian and Fu, 2014). Fire-

emitted aerosol in the ICP, is an important contributor to air pollution in Asia (Aouizerats et al., 2015; Streets et al., 2003), and is responsible for a large component of the atmospheric brown cloud (Ramanathan et al., 2007; Stone et al., 2007) and the regional precipitation (Huang et al., 2016; Yin, 2020).

Previous results indicated that fire emissions in ICP significantly impact the air quality in southern China (Chan et al., 2003; Huang et al., 2013; C.-Y. Lin et al., 2014; Zhang et al., 2022; Zhu et al., 2016). Engling et al. (2011) estimated the impacts of fire emissions from Southeast Asia on the concentrations of black carbon (BC) and particulate matter at a site in southern China during the biomass burning season in a specific year. Zhang et al. (2018) found that fire emissions in South and Southeast Asia had a significant impact on the $\text{PM}_{2.5}$ chemical composition at a site in southern China from 29 March to 27 April of 2012. The concentrations of aerosol and ozone in southern China were affected by the transport of fire emissions from the ICP region during a short period in the spring. Compared to ozone, the impact on aerosol concentration is greater (Deng et al., 2008; Xing et al., 2021). Past studies have shown that fire emissions from the ICP region contribute approximately 10–70 % of $\text{PM}_{2.5}$ in southern China (Fan et al., 2023; Li et al., 2017b; Q. Yang et al., 2022; Zhang et al., 2021; Zhu et al., 2022).

Besides the influence on the atmospheric environment, the smoke aerosol transported to southern China has a significant impact on the

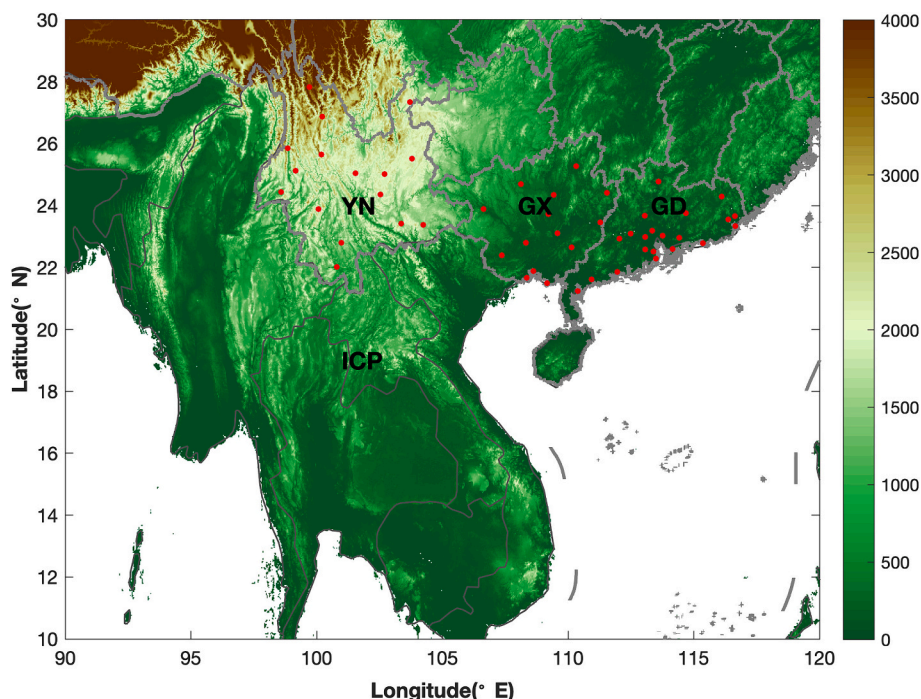


Fig. 1. Topography of the study regions and the 41 $\text{PM}_{2.5}$ ground-based stations from CMEE (red dots) for model evaluation.

weather and climate in the area (Chen et al., 2017; Ding et al., 2013; Huang et al., 2016). Ding et al. (2021) found that biomass smoke from Southeast Asia amplified the semi-direct effect of low clouds in the South China Sea through aerosol-boundary-layer-monsoon interactions. Xu et al. (2018) indicated the effect of biomass burning on BC in the Tibetan Plateau and the melt of snow and hydrologic resources. S. Yang et al. (2022) found strong influences of biomass burning aerosols on regional circulation and precipitation during the pre-monsoon season (Mar–Apr) in Southeast Asia and southern China. C.-Y. Lin et al. (2014) studied the long-range transport of Southeast Asia biomass-burning aerosols to Taiwan and their radiative forcings over East Asia, and found the influence of biomass-burning aerosol plume transported from ICP to southern China with a reduction in shortwave radiation of about 20 Wm^{-2} at the ground surface during March 15–18, 2008. Li et al. (2022) showed that fire in Southeast Asia induced a regional mean total radiative effect of 0.06 Wm^{-2} at TOA and caused 40 % precipitation decrease in north Vietnam and southern China during March 15 to April 15, 2019.

Above researches improved our understanding of the impact of fire emissions from Southeast Asia on southern China. However, most previous studies explored fire contributions based on 1–2 cases or for short periods. In addition, the impact was often analyzed at a single site, which may not represent the entire region. The multi-year contribution to aerosol concentration has been studied in previous works (Yin et al., 2019; Zhu et al., 2022). However, it is also important to quantify the multi-year contribution to aerosol radiation forcing, as it is related to the impact of smoke on the climate. To overcome these knowledge gaps, the objective of this work is to quantify the long-term contribution of ICP fire emissions transport to aerosol radiation forcing in three regions of southern China during 2013–2019 using models' simulations as well as ground and satellite observations. The three regions are Yunnan (YN), Guangxi (GX), and Guangdong (GD) from west to east, respectively.

2. Materials and method

2.1. Datasets

2.1.1. $PM_{2.5}$ and aerosol optical depth (AOD)

We used observed surface $PM_{2.5}$ concentration data from China's Ministry of Ecology and Environment (CMEE, <http://www.cnemc.cn/en/>) and AOD at 550 nm from the Moderate Resolution Imaging Spectroradiometer (MODIS, <https://www.earthdata.nasa.gov/>) during March–May from 2013 to 2019 for the GEOS-Chem chemical transport model and the Column Radiation Model (CRM) validations, respectively. Fig. 1 shows the study regions and the 41 ground stations for $PM_{2.5}$ from CMEE for model evaluation. The study regions in this work mainly include Yunnan (YN), Guangxi (GX), and Guangdong (GD) provinces in southern China, as well as the neighboring ICP region. Since biomass burning events occur more frequently in spring (March–May) in Southeast Asia (which can be transported to southern China and have an important impact on the environment and climate of the region), this study specifically focuses on the spring season. The 41 $PM_{2.5}$ sites in China are selected based on the administrative divisions of provinces. Past studies have shown that the data from the CMEE stations fit Benford's Law and were highly consistent with the data measured by the U.S. Embassy in China since 2013 (Liang et al., 2016; Stoerk, 2016). We use hourly concentrations of $PM_{2.5}$ at the 41 stations in the YN, GX, and GD regions to validate the aerosol concentrations simulated from the GEOS-Chem model at the site and on monthly scales. The MODIS instruments onboard Aqua and Terra view the whole Earth's surface every 1–2 days with a 2330 km swath at 36 spectral bands. The monthly $1 \times 1^\circ$ grid average of Dark-Target/Deep-Blue combined AOD at 550 nm data from MODIS Collection 6.1 are used to validate the AOD simulated by the CRM model at regional, monthly, and annual scales.

2.1.2. Fire emissions

The Global Fire Emissions Database version 4.1 (GFED4s) (van der Werf et al., 2017) was analyzed and used as fire emissions inventory for simulations. The GFED4s derives biomass burned based on satellite retrieval of burned areas and active fire information (Giglio et al., 2013). GFED4s considers six land cover types: temperate forest, peat, savanna, deforestation, boreal forest, and agricultural waste. For each land type, fire-induced emissions were estimated as the product of dry matter and species-specific emission factors from Akagi et al. (2011). By default, GFED4s provides monthly fire emissions with a spatial resolution of 0.25° from 1997 to the present. Since 2003, daily fire emissions data have been available by multiplying daily scale factors with monthly emissions data (Mu et al., 2011).

2.2. Models

2.2.1. GEOS-Chem model

The 3-D GEOS-Chem (<http://wiki.seas.harvard.edu/geos-chem/>) chemical transport model version 12.0.0, with $2^\circ \times 2.5^\circ$ horizontal resolution and 47 layers from the surface to 0.01 hPa for the vertical grid (Bey et al., 2001), was used to estimate fire-induced aerosol. The model was driven by the Global Modeling and Assimilation Office MERRA-2 meteorology, with a temporal resolution of 3 h for meteorological parameters and 1 h for surface fields. The model included a fully coupled O_3 - NO_x -hydrocarbon-aerosol chemical mechanism to simulate atmospheric composition and air quality (Gong and Liao, 2019; Lei et al., 2020). All GEOS-Chem emissions were configured at runtime using the Harvard–NASA Emission Component module described by Keller et al. (2014). The default global anthropogenic emissions were overwritten over East Asia by the MIX inventory (Li et al., 2017a). The biomass burning inventory was adopted from GFED4s. GEOS-Chem used the TPCORE advection algorithm proposed by Lin and Rood (1996). Convective transport was computed from convective mass fluxes in the meteorological fields, as described by Wu et al. (2007). The boundary layer mixing in GEOS-Chem used the nonlocal scheme implemented by Lin and McElroy (2010). Dry deposition was based on Wesely (1989), and aerosol deposition was based on Zhang et al. (2001). Wet deposition was performed as previously described by Liu et al. (2001). Studies have shown that GEOS-Chem captures the spatiotemporal variability of $PM_{2.5}$ in China (Dang and Liao, 2019).

2.2.2. Radiative transfer model

The Column Radiation Model (CRM) is the standalone version of the radiative transfer module used by the NCAR Community Climate Model (<http://www.cesm.ucar.edu/models/>). In this model, aerosol radiative effects, including absorbing and scattering processes, are calculated at 20 vertical layers from the surface to 0.5 hPa at hourly intervals (Yue and Unger, 2017). The CRM utilizes aerosol profiles of all species simulated by GEOS-Chem, including sulfate, nitrate, BC, organic carbon (OC), dust (clay and silt), and sea salt (coarse and accumulation modes). Aerosol optical parameters (e.g., single scattering albedo (SSA), extinction coefficients (m^2/g), and asymmetric parameters) are adopted from Yue and Liao (2012) for sea salt, Yue et al. (2010) for mineral dust, and the RegCM4 model for other species (Giorgi et al., 2012) based on Mie scattering processes. Some aerosol optical parameters were shown in the supplement by Yue and Unger (2017). These parameters vary with changes in both wavelength and relative humidity. Sulfate and nitrate aerosols share the same parameters. For carbonaceous aerosols (BC and OC), hydrophobic and hydrophilic are considered separately. The aerosol internally mixed method is used in the CRM model. In this study, the CRM is used to simulate aerosol-induced perturbations in net radiative fluxes at the surface and top of the atmosphere. The model is driven by hourly $1 \times 1^\circ$ meteorology from MERRA-2 reanalysis and 3-hourly cloud cover and liquid water path from CERES SYN1deg (<http://ceres.larc.nasa.gov/>). Zhou et al. (2022) have clarified that CRM driven with aerosol concentrations from GEOS-Chem showed similar patterns

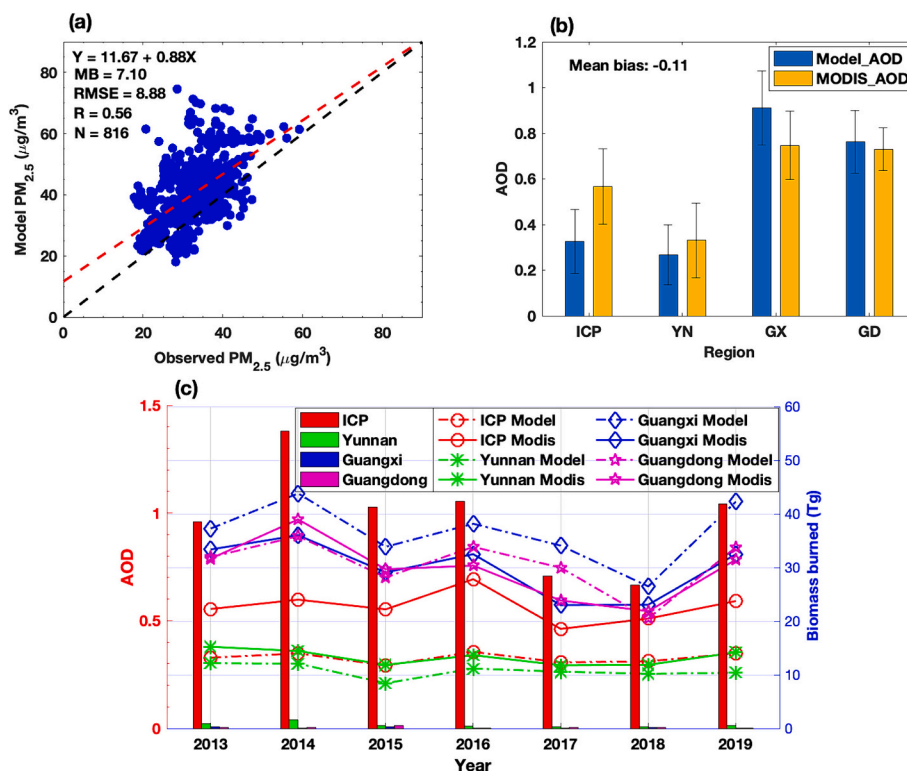


Fig. 2. Models evaluation of simulated PM_{2.5} and AOD using ground-based observation and satellite MODIS observation during March–May from 2013 to 2019: (a) GEOS-Chem monthly PM_{2.5} evaluation by ground observation from CMEE at the 41 sites; (b) CRM regional monthly AOD evaluation using MODIS AOD; (c) annual AOD change assessment. The dots in (a) are the spatial-temporal matching of monthly PM_{2.5} and the statistical parameters include the number of matchup data (N), the slope and intercept at the y axis of the linear regression (red line), the mean bias (MB), the root-mean-squared error (RMSE), and the correlation coefficient (R). The regional monthly mean bias of AOD is shown in (b). The lines in (c) are the regional annual AOD and bars are the monthly averaged biomass burned in each region.

of shortwave radiation to the satellite observations with correlation coefficients larger than 0.9.

2.3. Model simulations

We perform GEOS-Chem and CRM runs to explore the radiative impacts of fire emissions. We initially conduct three GEOS-Chem model runs to obtain three-dimensional concentrations of different aerosol

types, including sulfate, nitrate, OC, BC, dust, and sea salt, which are driven with the same meteorology and emissions except the fire emissions. “Fire”, “Nofire”, and “NofireICP” represent the model simulations with global fire, without global fire, and without fire emissions in the ICP region, respectively. Then, the CRM runs aim to calculate aerosol-induced optical and radiative changes using aerosol profiles simulated by GEOS-Chem. The CRM runs provide aerosol optical properties (AOD and SSA) and radiative flux in all-sky conditions (which are forced with

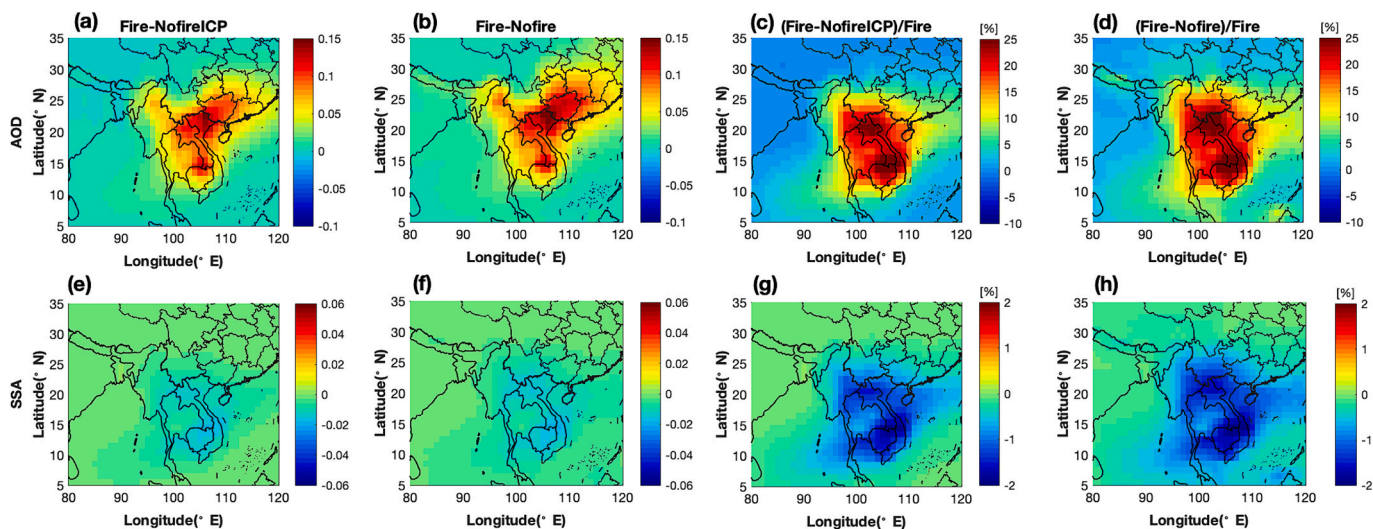


Fig. 3. The absolute (a, b, e, f) and relative (c, d, g, h) contributions of ICP (Fire-NofireICP) and global (Fire-Nofire) fire to AOD (top) and SSA (bottom) at 550 nm during the spring of 2013–2019.

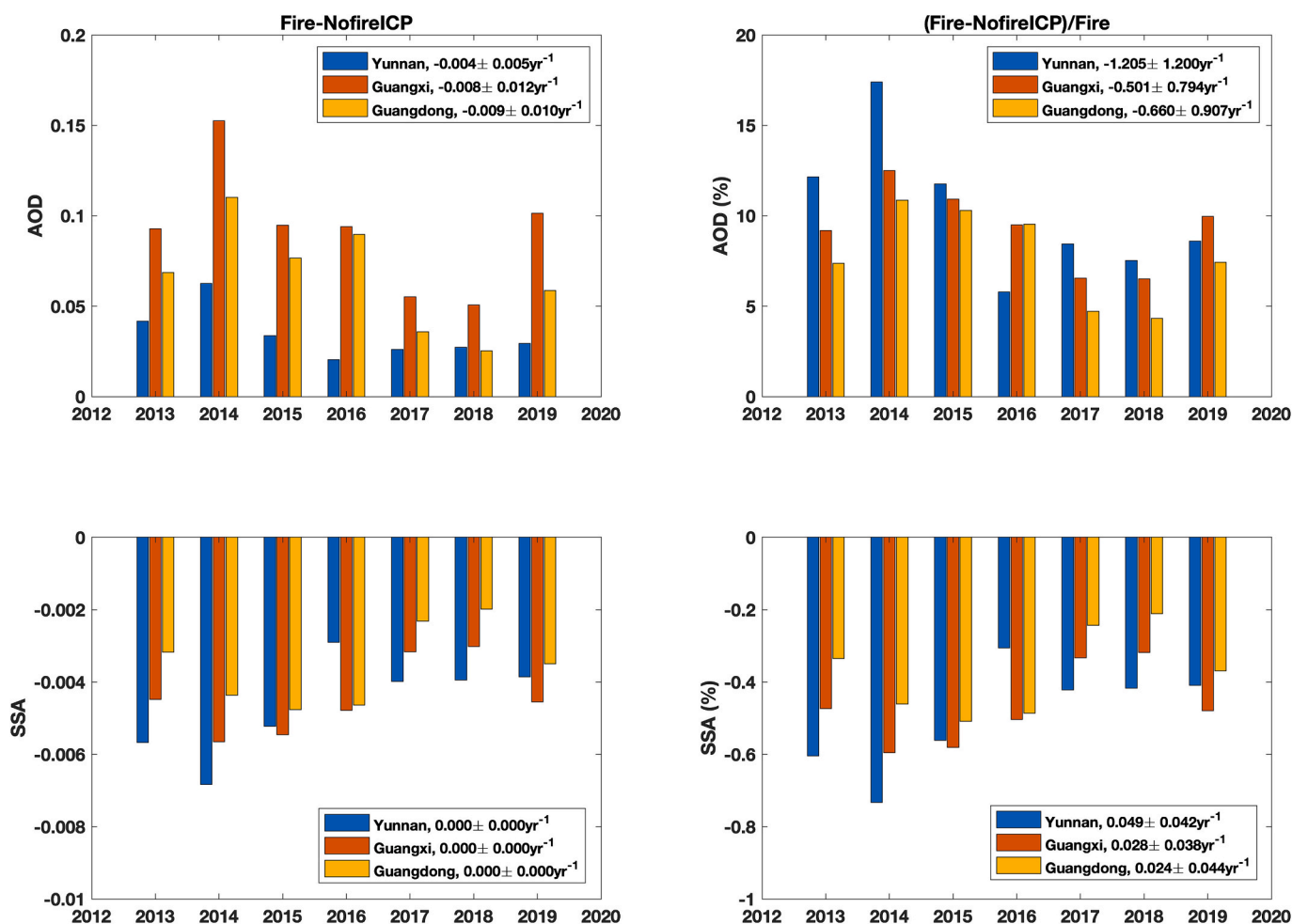


Fig. 4. The annual change of the absolute (left) and relative (right) contributions of fire emissions in the ICP region to AOD (top) and SSA (bottom) at 550 nm in the three southern provinces of China in the spring during 2013–2019. The values in the legends show the trends (mean ± standard) with the p value < 0.1 .

observed cloud profiles) and clear-sky conditions (forced without any cloud coverage) at the surface and top of the atmosphere. The differences between “Fire” and “Nofire” represent the contributions of global fire emissions, while the differences between “Fire” and “NofireICP” represent the contributions of ICP fire emissions. These differences divided by “Fire” indicate the relative contributions of fire emissions.

3. Model evaluation

Fig. 2 shows the evaluations of model simulations at the scales of the site, regional (monthly), and annual changes. Compared to the observed $\text{PM}_{2.5}$ at the sites (Fig. 2a), the GEOS-Chem $\text{PM}_{2.5}$ shows a relatively high correlation of 0.56 with the observed monthly $\text{PM}_{2.5}$, but slightly overestimates the surface monthly $\text{PM}_{2.5}$ over the study area with MB of $7.10 \mu\text{g}/\text{m}^3$. Compared to MODIS monthly AOD at the four study regions (Fig. 2b), CRM AOD agrees well with the regional variation observed by MODIS with high values in the GX and GD and low values in the ICP and YN regions. However, the model generally underestimates the AOD with a monthly regional mean bias of -0.11 , especially for the undervaluation in the ICP region. These may be related to the possible error in the vertical distribution of aerosols, which is not considered in this work. As for the annual changes (Fig. 2c), both the model and MODIS AOD show increases in 2013–2014, 2015–2016, and 2018–2019, while decreases in 2014–2015 and 2016–2018 over almost all study regions. Besides, these annual variations of AOD are highly consistent with the annual changes in biomass burned in the study region, especially in the ICP region, where biomass burned is much higher than that in the other three

regions of southern China. The model underestimates the AOD over the ICP region with a bias of about -0.2 . However, over the three regions in southern China, the biases are < 0.1 compared to satellite-based observations. Overall, the GC and CRM models reasonably capture the temporal and spatial distribution of surface aerosol concentrations and column aerosol optical properties over the study regions during the spring of 2013–2019.

4. Results

4.1. Contributions of fire in ICP to aerosol properties

4.1.1. Contributions to AOD and SSA

AOD and SSA are two major optical parameters to estimate aerosol radiation forcing. The absolute and relative contributions of ICP region (Fire-NofireICP) and global (Fire-Nofire) fire emissions to AOD (top) and SSA (bottom) at 550 nm are quantified by GEOS-Chem and CRM model simulations (Fig. 3). As for AOD, the results indicate that the fire emissions over the ICP region could contribute > 0.15 (absolute) and 25 % (relative) of the AOD during the spring of 2013–2019 in and around the north of Laos and Vietnam, where biomass burning is also highly frequent. The absolute and relative contributions to the three regions of China are different, with the highest absolute contribution (> 0.1) in the GX region but the highest relative contribution ($> 15\%$) in the YN region. The impact of ICP fire emissions on SSA over the four regions is negative because fire emits more absorptive aerosols. The light absorption due to brown carbon from fire emissions has been recognized as

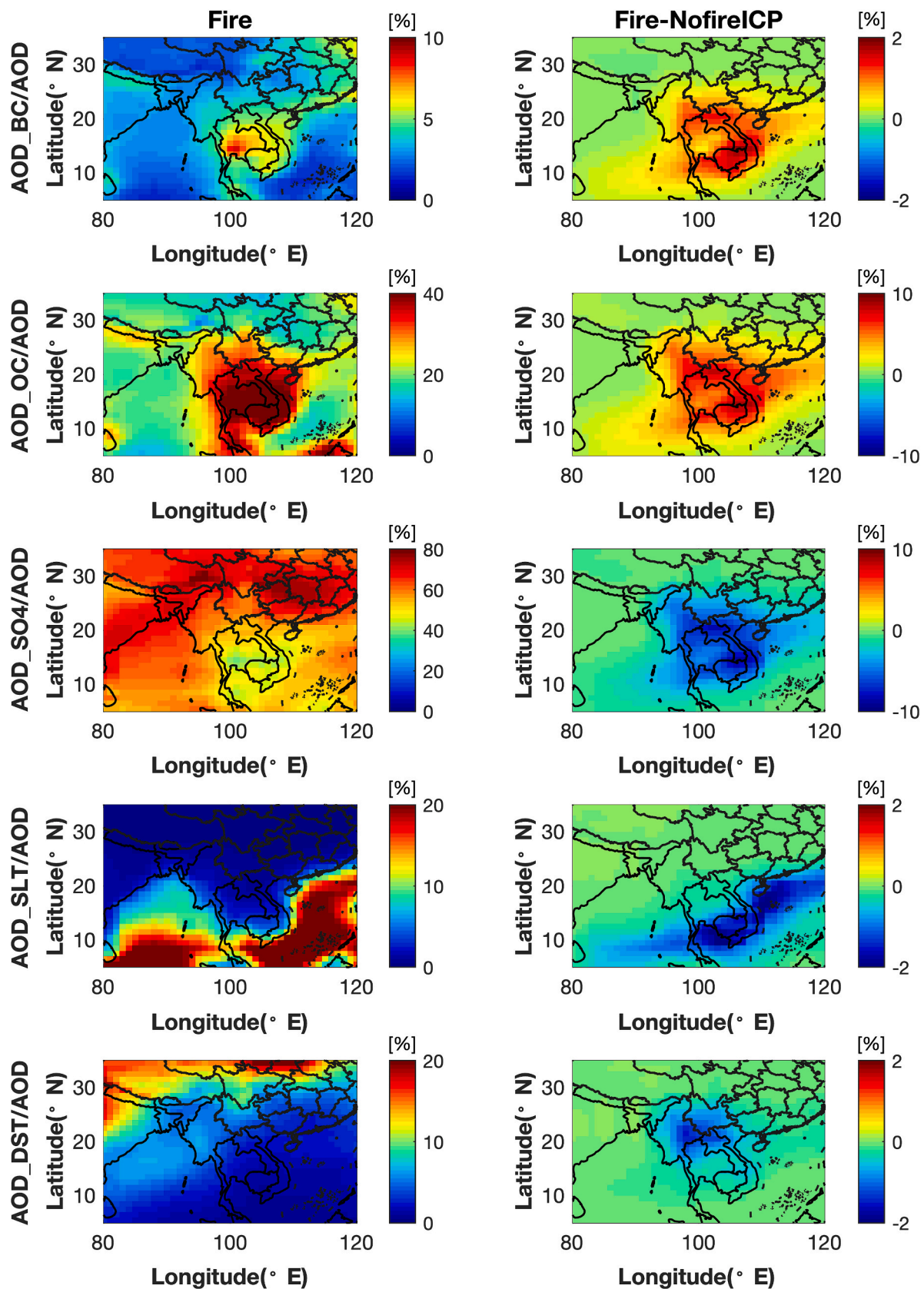


Fig. 5. The proportions of five aerosol types in total AOD for the model simulations with fire (the left column), and the contributions of ICP fire (Fire-NofireICP) (the right column) to the proportions of the five aerosol types.

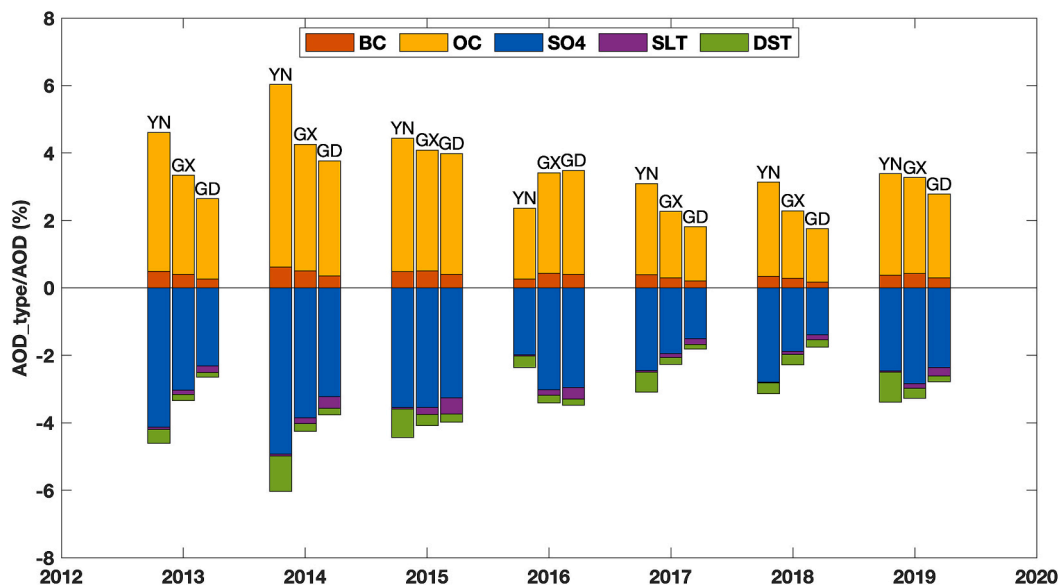


Fig. 6. The annual change of the ICP fire contributions to the proportions of five aerosol types in total AOD in the three southern provinces of China in 2013–2019 spring.

important contributor to total aerosol absorption (more than ~25 % of BC), but the contribution may decrease along transport associated with photo-bleaching (Zhang et al., 2019; Zhao et al., 2015). Thus, the results show that the absolute and relative contributions to SSA in the spring are less than -0.05 and -2 %, and their high impact areas are consistent with the impact area of AOD. Comparing Fig. 3(c) and (d), Fig. 3(g) and (h) (that is ICP fire contributions and the global fire contributions), it can be found that the contributions of global fire to AOD and SSA are similar to those of ICP fire emissions, with a slightly larger area of influence and a slightly higher contribution value, which indicates the ICP region is the primary source of fire emissions over the study regions. Therefore, the contributions of ICP fire emissions are the focus of the subsequent content.

The annual changes in contributions of ICP fire emissions to AOD and SSA in the southern Chinese regions (Fig. 4) illustrate the largest absolute and relative values in 2014 and the minimums in 2018. These annual variations in the contributions of fire aerosols from the ICP to AOD and SSA in the south-three regions of China are consistent with the annual biomass burned in the ICP region (Fig. 2c). These suggest that the annual changes in the contributions to southern China are affected by the yearly fire activities in the ICP region. From 2013 to 2019, the general trends of ICP fire impacts on AOD and SSA in the southern Chinese regions are declined. Due to the low values (<0.008), the trends of SSA are <0.0005 . The fastest declined trend of absolute contribution is shown in the GD region ($-0.009 \pm 0.010 \text{ yr}^{-1}$ for AOD), while the trends of relative contribution demonstrate the maximum descent speed

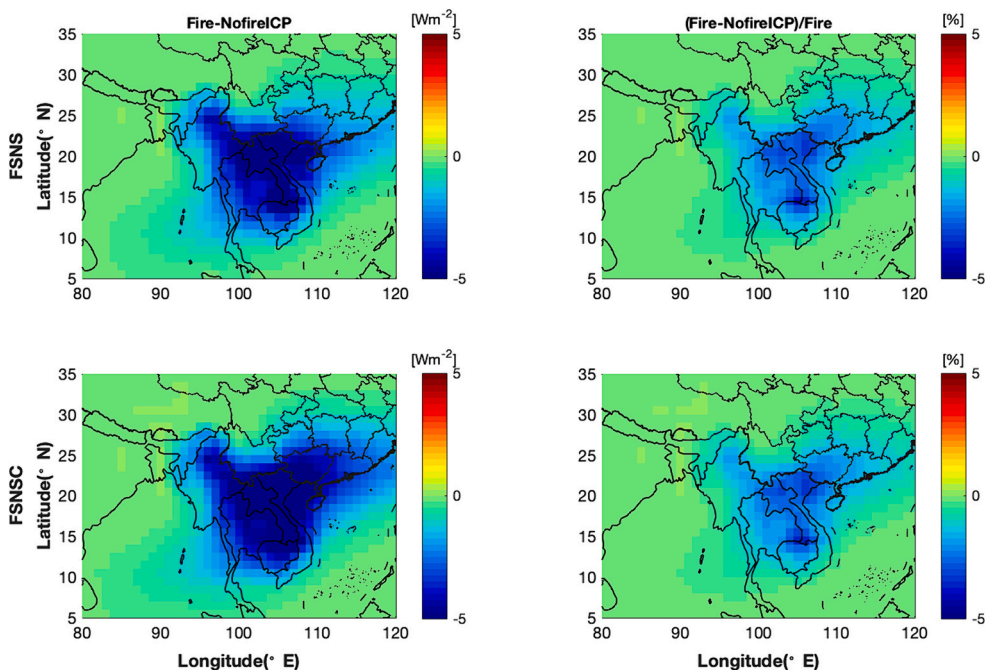


Fig. 7. The absolute (Fire-NofireICP, column 1) and relative ((Fire-NofireICP)/Fire, column 2) contributions of ICP fire to net shortwave radiation at the surface in all sky (FSNS) and clear sky (FSNSC).

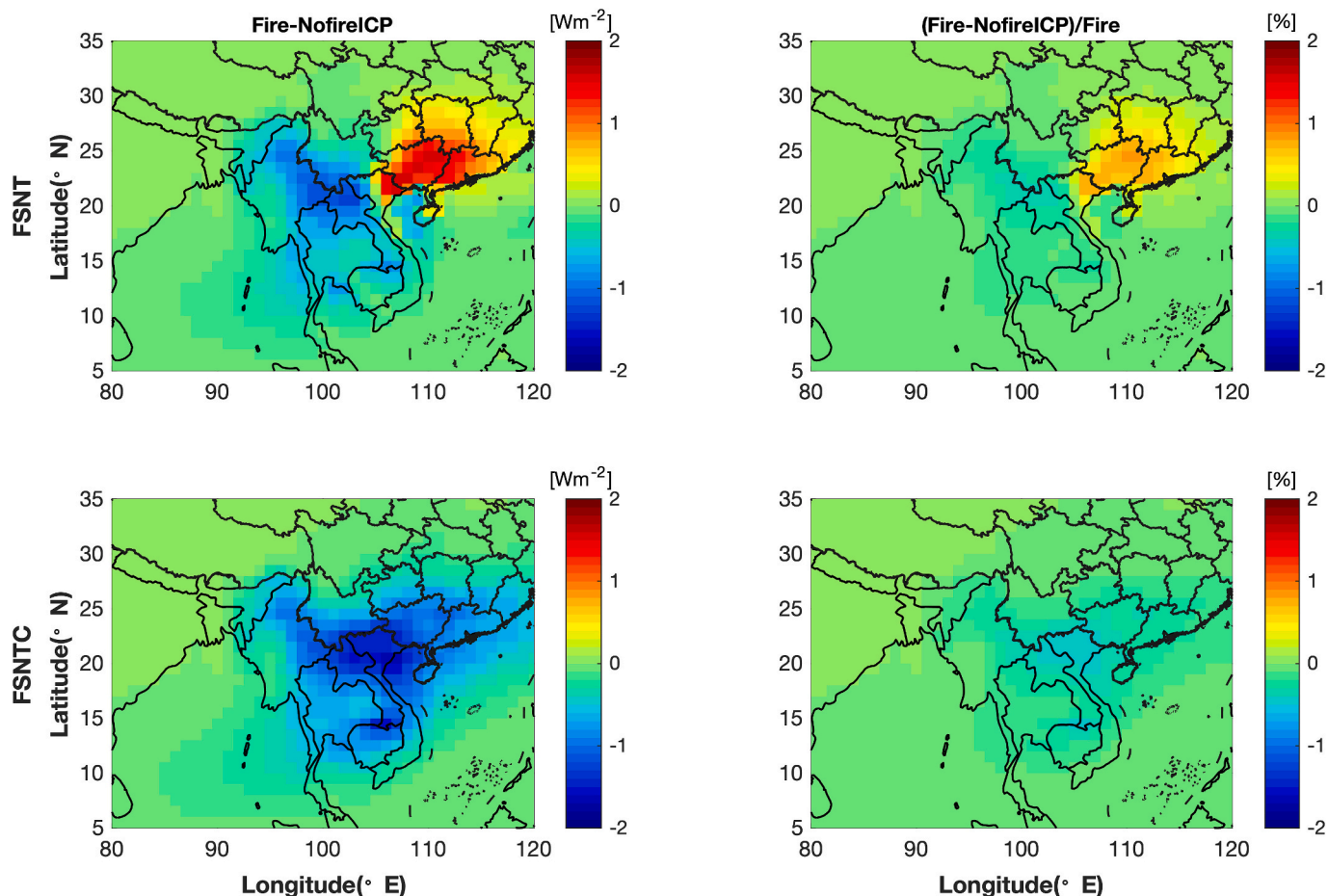


Fig. 8. The absolute (column 1) and relative (column 2) contributions of ICP fire to net shortwave radiation at the top of atmosphere in all sky (FSNT) and clear sky (FSNTC).

in the YN region ($-1.205 \% \pm 1.200 \% \text{ yr}^{-1}$ for AOD and $0.049 \% \pm 0.042 \% \text{ yr}^{-1}$ for SSA).

4.1.2. Contributions to proportions of aerosol types

The AOD and SSA further depend on the chemical composition, the reflective index for each component, size distribution, and mixing state (Tuccella et al., 2020). To assess the impact of fire emissions on aerosol components, Fig. 5 shows the proportions and fire contributions of five aerosol types in total AOD. The five aerosol types are BC, OC, sulfate+nitrate+ammonium (SO₄), sea salt (SLT), and dust (DST) aerosols. In the study regions, SO₄, OC, and BC are the dominant aerosol types, while the proportions of SLT and DST are minimal. The fire emissions in the ICP lead to increases in the proportions of BC and OC and decreases in the other three aerosol types. The increase in OC (up to about 10 %) is about 5 times that of BC (up to about 2 %) and comparable to the reduction of the proportions of SO₄ (up to about -10 %) in the ICP region. As for the other three regions located in the downstream area of ICP fire emissions, the trends of the proportion of the three major aerosol types agree with those in the ICP region, but the magnitude is less than half of that in the ICP. The regional means of the three regions in southern China show increases in the proportions of BC by $0.4 \% \pm 0.1 \%$ and OC by $3.0 \% \pm 0.9 \%$. Besides, the percentage of influence in YN is larger than that in the GX and GD regions. As for annual changes (Fig. 6), the variability in the increase of OC and BC types is consistent with the annual biomass burned in the ICP region. Besides, the ICP fire contributions to the proportions of BC and OC types in total AOD also showed downward trends in the three southern provinces of China during the 2013–2019 spring.

4.2. The aerosol radiation effect of fire emissions from the ICP region

4.2.1. The contributions to net shortwave radiation flux

The aerosol radiative forcing of fire aerosols in the biomass burning season is important for climate change. Fig. 7–9 illustrates the absolute and relative contributions of ICP fire to the net shortwave radiation flux for the surface, top of the atmosphere, and the atmosphere. During the spring season of 2013–2019, ICP fire aerosols decrease net shortwave radiation reaching the surface (FSNS, Fig. 7) up to -5 Wm^{-2} in the local (ICP) and downwind regions at all sky, which account for $-2 \% \sim -5 \%$ of the FSNS. In the clear sky (FSNSC), the reduction values in FSNSC are higher, with values reaching up to -8 Wm^{-2} . As for the net shortwave radiation at the top of the atmosphere (Fig. 8), fire aerosols from the ICP region cause a perturbation in the study regions in the all sky (FSNT), with negative changes in the ICP and YN regions (up to -1 Wm^{-2} , -0.5%), but positive changes in the GX and GD regions (up to 2 Wm^{-2} , 1%), which may be related to the complex effects of clouds and aerosols (Ding et al., 2021; Huang et al., 2023). However, in the clear sky (FSNTC), the fire aerosols from the ICP region only reduce the FSNTC in the study regions without any positive effect. In addition, the negative contributions (-2 Wm^{-2}) are larger than those in the all sky. The average contributions of ICP fire to the net shortwave radiation flux of the atmosphere are significant (Fig. 9). The fire emissions from the ICP region heat the atmosphere by about 5 Wm^{-2} (5 %) in both the local (ICP) and downwind regions in all sky (FSNA) and clear sky (FSNAC). The increase of BC and OC aerosols (Fig. 5), especially BC, can absorb solar shortwave radiation, reduce the SSA (Fig. 3), and lead to heating the atmosphere (Fig. 9). The aerosol radiative forcing effects may be

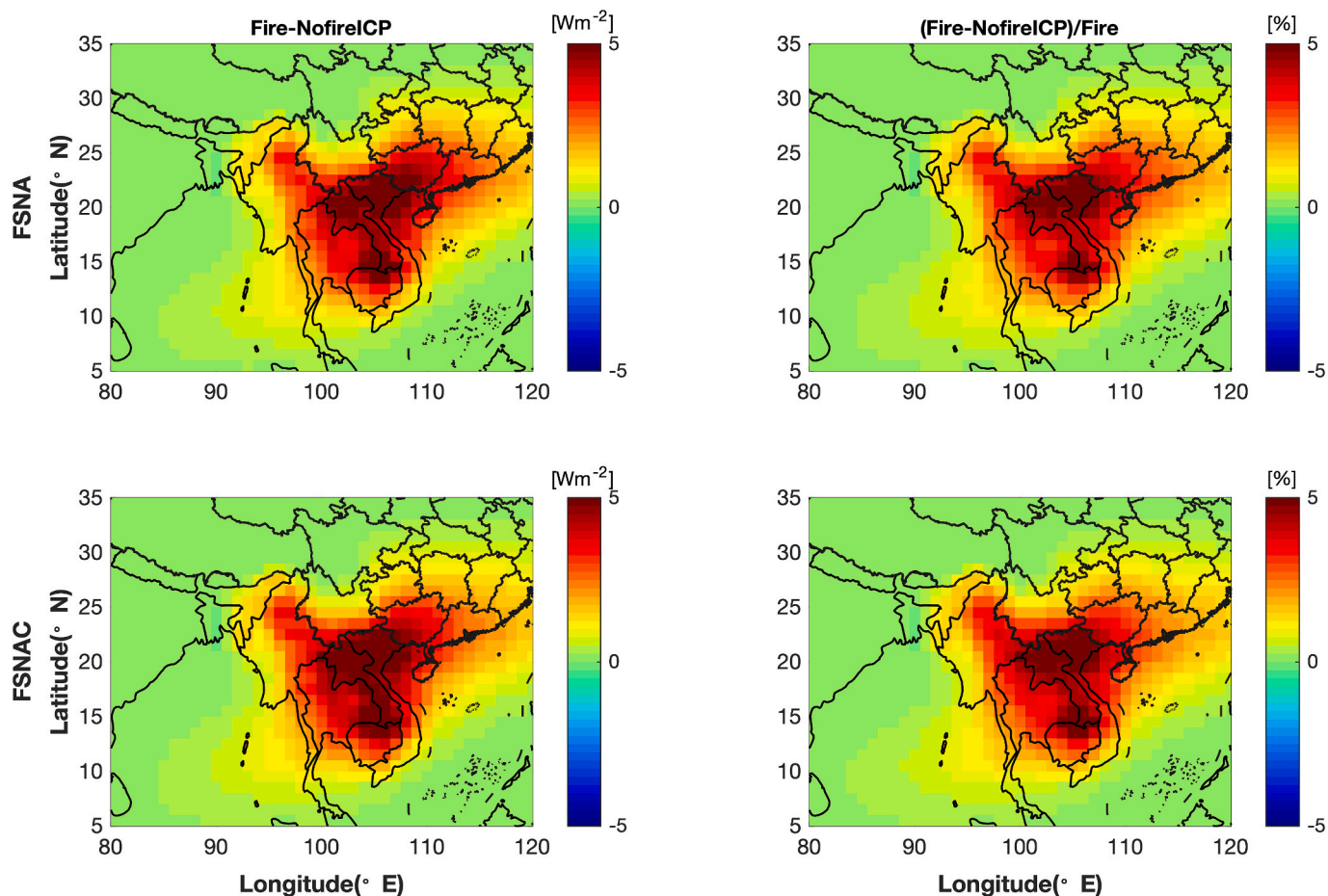


Fig. 9. The absolute (column1) and relative (column 2) contributions of ICP fire to the net shortwave radiation in the atmosphere in all sky (FSNA) and under clear sky (FSNAC).

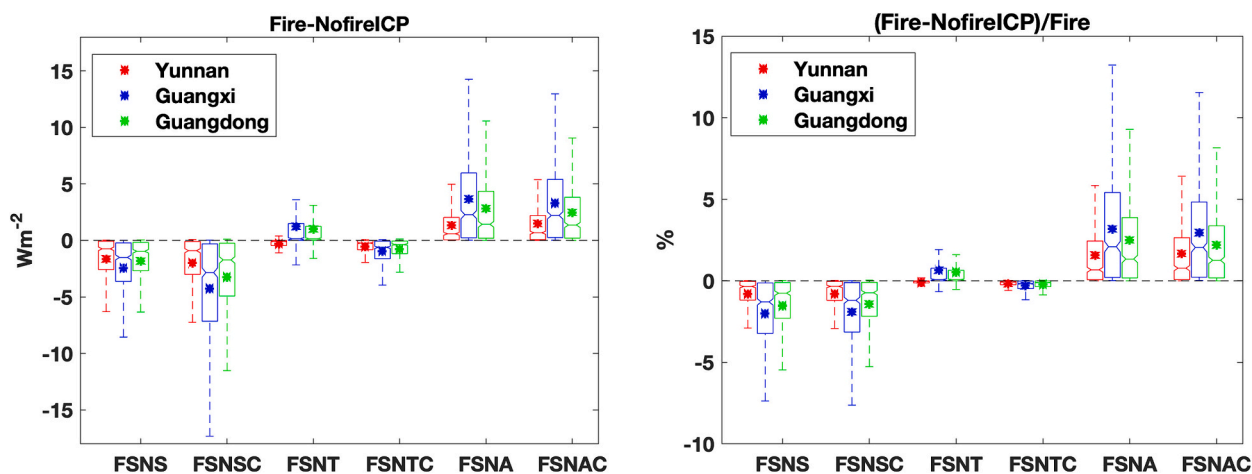


Fig. 10. The box plots of the daily absolute (Fire-NofireICP) and relative ((Fire-NofireICP)/Fire) contributions of fire emissions from the ICP region to the net shortwave radiation in the three southern regions of China during 2013–2019 spring.

influenced by the size distribution and mixing state (Han et al., 2013; Pilinis et al., 1995), but these are not the focus of this work. The contributions of fire emission to aerosol longwave radiation in the study regions are also assessed. However, the contributions are very small, with absolute value of about 10^{-6} Wm^{-2} . Therefore, this study only focuses on the contribution to shortwave radiation.

4.2.2. The contributions to the southern regions of China

To clearly qualify the impact of ICP on net shortwave radiation in the three southern regions of China, Fig. 10 displays the boxplots of the daily absolute and relative contributions of fire aerosols from the ICP region to the three southern regions of China during 2013–2019 spring. The impacts of ICP fire aerosols on the surface radiation (means up to -5 Wm^{-2}) and the atmosphere (means up to 5 Wm^{-2}) are higher than those

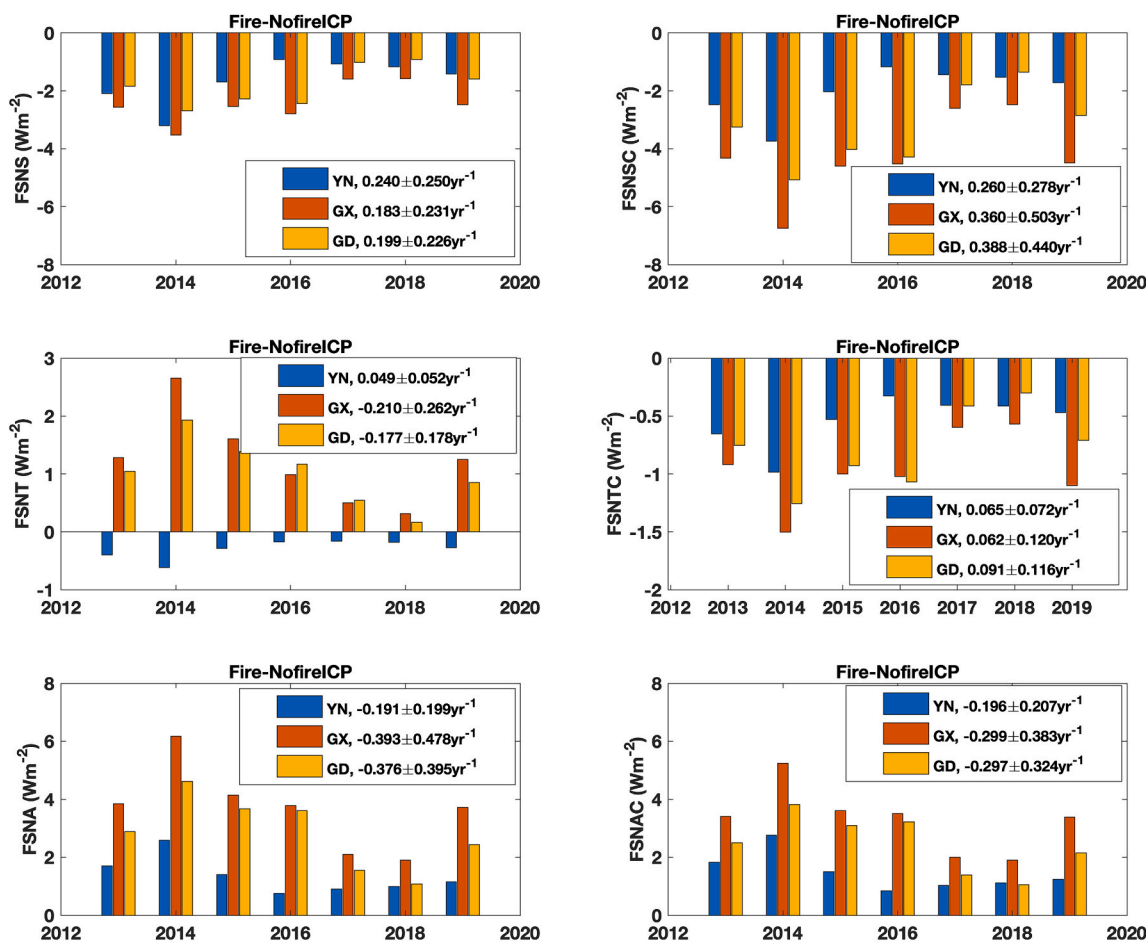


Fig. 11. The annual change of the absolute contributions (Fire-NofireICP) of fire emissions from the ICP region to the net shortwave radiations in the three southern regions of China during 2013–2019. The values in the legends show the trends (mean ± standard) with the p value < 0.1.

at the top of the atmosphere (means up to $-1-1 \text{ Wm}^{-2}$). Regionally, the ICP fire contributions in the GX are higher than those in the YN and GD regions, which is proportional to the contribution to aerosol loading (Fig. 3a). As for the daily variations, the daily fire absolute contribution from the ICP region to the FSNSC in the GX region can exceed -15 Wm^{-2} , which is comparable to the case study in C.-Y. Lin et al. (2014), and the relative contribution can be up to about -8% in the FSNS and FSNSC in the GX region. Compared to the GX region, the daily contribution in YN is lower, with value of about -6 Wm^{-2} (-3%) in the FSNS, while the daily contribution in GD is higher than in YN, with high values larger than -10 Wm^{-2} in the FSNSC and -5% in the FSNS and FSNSC. The contributions to those at the top of the atmosphere in the southern three regions of China are low, but the contributions to the atmosphere are higher, with daily contributions of larger than 10 Wm^{-2} (10%) in the GX and GD regions and 5 Wm^{-2} (5%) in the YN region.

The absolute contribution of about -5 Wm^{-2} to radiation fluxes is likely lower than in previous studies (Li et al., 2022; C.-Y. Lin et al., 2014). The reason is that this contribution in this work represents the regional average over multiple years rather than a short period at a site. We have selected the regional pollution days during the biomass season from 2015 to 2019 in the YN region (Zhu et al., 2022). The statistical results of the contributions could be more than twice the multi-year mean (that is the contribution of ICP fire to southern China on the polluted day is comparable with the previous studies), which also indicates the impact of ICP fire emissions on heavy biomass burning days in southern regions of China can reach a high level.

4.2.3. The annual change in the contributions to the southern China

Figs. 11 and 12 illustrate the annual changes in the absolute and relative contributions of fire emissions from the ICP region to net shortwave radiation in the three southern regions of China during the spring of 2013–2019. Both the absolute and relative impacts reached their peaks in 2014. Furthermore, the contribution values exhibited a decline from 2014 to 2018 with a small fluctuation in 2015 and 2016, followed by an increase from 2018 to 2019. These annual variations in the contributions of fire aerosols from the ICP to the net shortwave radiation in the southern three regions of China are also consistent with the yearly biomass burned in the ICP region (Fig. 2c). From 2013 to 2019, the general trend of impact on the net shortwave radiation at the surface, top of the atmosphere, and the atmosphere in the southern three regions of China from ICP fire declined. As for the absolute contributions, the annual contributions to the FSNS show the largest trend in the YN region ($0.240 \pm 0.250 \text{ Wm}^{-2} \text{ yr}^{-1}$), while the contributions to the FSNSC show the largest trend in the GD region ($0.388 \pm 0.440 \text{ Wm}^{-2} \text{ yr}^{-1}$). The trends in contributions to radiation at the top of the atmosphere are the biggest in GX for the FSNT ($0.210 \pm 0.262 \text{ Wm}^{-2} \text{ yr}^{-1}$) and in GD for the FSNTC ($0.091 \pm 0.116 \text{ Wm}^{-2} \text{ yr}^{-1}$). The declined trends of heating the atmosphere are highest in GX for the FSNA ($0.393 \pm 0.478 \text{ Wm}^{-2} \text{ yr}^{-1}$) and FSNA ($0.299 \pm 0.383 \text{ Wm}^{-2} \text{ yr}^{-1}$). As for the relative contributions (Fig. 12), the trends in different regions are basically similar to those of the absolute contributions.

To explore the relationship between the variations of impact on the aerosol properties and aerosol radiation forcing and the changes in fire emissions, Table 1 shows the correlations (R) of biomass burned in ICP and its absolute contributions to aerosol radiation forcing and properties

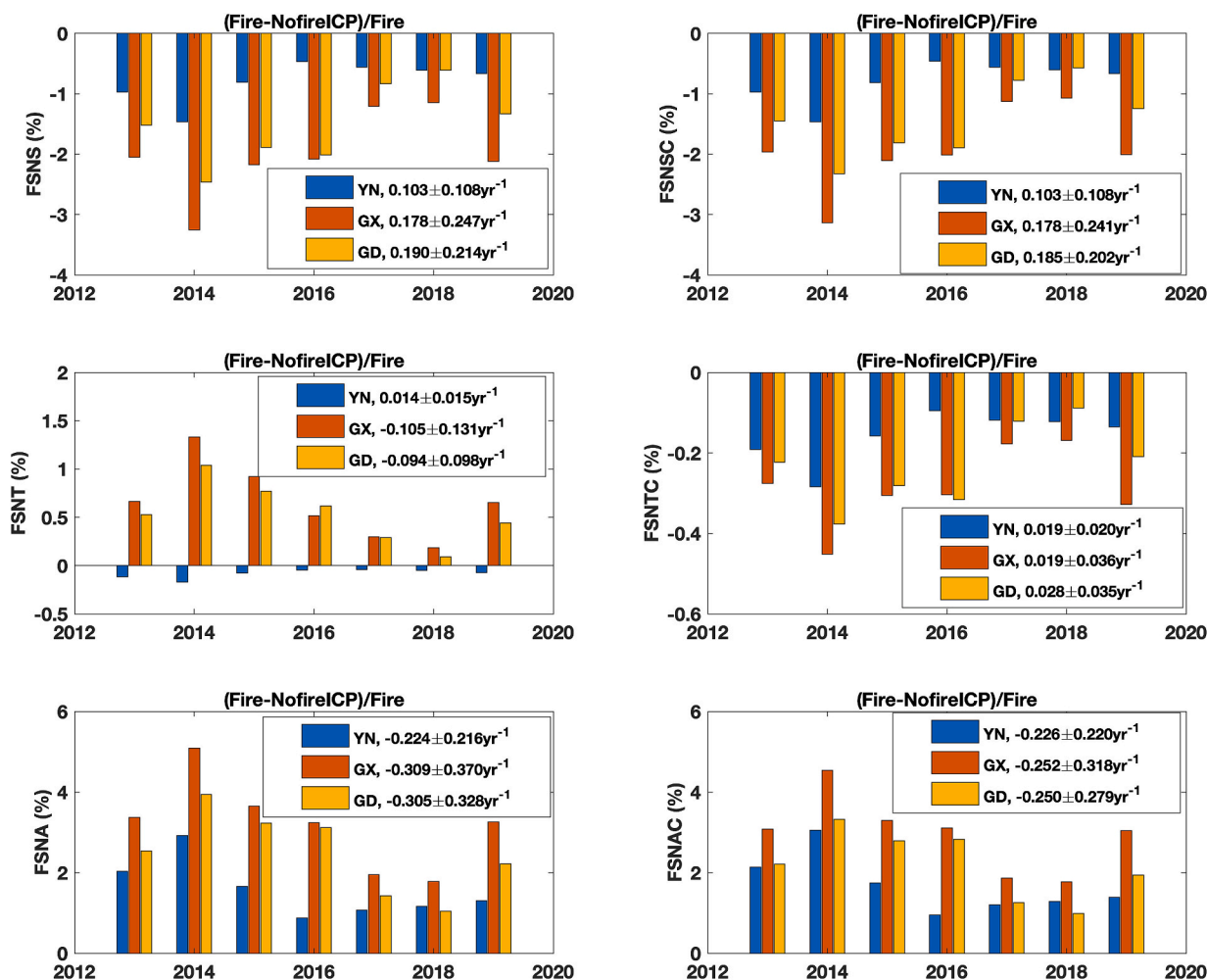


Fig. 12. The annual change of the relative contributions ((Fire-NofireICP)/Fire) of fire emissions from the ICP region to the net shortwave radiations in the three southern regions of China during 2013–2019. The values in the legends show the trends (mean ± standard) with the p value <0.1.

Table 1

The correlations (R) of biomass burned in ICP and its absolute contribution to aerosol radiation forcing and properties in the three regions of China during 2013–2019.

Region	FSNS	FSNSC	FSNT	FSNTC	FSNA	FSNAC	AOD	SSA	Mean
YN	0.751	0.723	0.797	0.722	0.737	0.723	0.704	0.571	0.716
GX	0.985	0.996	0.947	0.995	0.985	0.992	0.990	0.923	0.977
GD	0.908	0.935	0.946	0.946	0.938	0.930	0.950	0.809	0.920

in the three regions of China during 2013–2019. The mean values of R between the biomass burned in ICP and the contribution are 0.716, 0.977, and 0.920 in the YN, GX, and GD regions, respectively. All values are >0.5, indicating the variation of these contributions could be largely explained by the changes in fire emissions in ICP. On the other hand, the values are <1.0, which suggests the variations in these contributions are affected not only by fire emissions but also by other factors such as transport or topography.

The results revealed the multi-year mean contributions of fire emissions to the aerosol properties and aerosol radiation forcing in the southern three regions of China during the biomass burning season (spring) of the neighboring ICP region. Such radiative perturbations of ICP fire emissions were expected to influence regional meteorology in southern China and should be considered in the climate simulations. Besides, the quantification of the fire contribution helped to improve understanding of the climate effects of smoke aerosols.

5. Conclusion and discussion

Combing the GEOS-Chem and CRM model simulations, the impacts of ICP fire emissions on aerosol properties and aerosol radiation forcing in the southern three regions of China during the spring season from 2013 to 2019 were analyzed. The main conclusions are as follows:

- (1) The fire emissions in the ICP region increased the AOD value by 0.1 (15 %) and decreased the SSA in the southern three regions of China during the spring season from 2013 to 2019. These impacts were attributed to increases in the proportions of BC (0.4 % ± 0.1 %) and OC (3.0 % ± 0.9 %) aerosol types.
- (2) The smoke aerosol transport from ICP fire emissions cooled the surface and heated the atmosphere in the southern regions of China, with the largest mean contributions to surface shortwave radiation forcing of -5 Wm^{-2} (-3 %) and daily contributions to the atmosphere radiation forcing of about -15 Wm^{-2} (-15 %) in the GX region, followed by the GD and YN regions.
- (3) The general trends of impact on the aerosol properties and

aerosol radiation forcing declined during 2013–2019, with the highest rate found in GX for the FSNA of $0.393 \pm 0.478 \text{ Wm}^{-2} \text{ yr}^{-1}$. Besides, the yearly changes in the contributions were consistent with the annual biomass burned in the ICP region.

This work quantified the multi-year mean contributions of fire emissions to the aerosol properties and aerosol radiation forcing in the southern three regions of China during the biomass burning season (spring) of the neighboring ICP region. The model simulations may exist uncertainties, such as model resolution, aerosol mixing state, and aerosol profile (Choi and Chung, 2014). What's more, the uncertainty of these contributions largely depends on the aerosol source inventories (fire emissions inventories and other aerosol emission inventories). The underestimate of simulated AOD in the ICP region may be related to the anthropogenic aerosols, which may not be well represented in the model. Therefore, further studies are required to quantify the impacts of the physicochemical processes of biomass burning aerosols and anthropometric aerosols on air quality and climate in these regions.

Data Availability.

The 41 stations of PM_{2.5} data are obtained from China's Ministry of Ecology and Environment (<http://www.cnemc.cn/en/>). The MODIS AOD data can be downloaded from <https://www.earthdata.nasa.gov/>. The GEOS-Chem model code and shared data, including GFED inventory, are available online (http://wiki.seas.harvard.edu/geos-chem/index.php/Main_Page). The CRM model is available from <http://www.cesm.ucar.edu/models/>.

Author contribution

All authors help to shape the ideas and review this manuscript. JZ and XY designed, and wrote the manuscript; JZ and HZ carried out the models' simulations; JZ, XY, and HZ help to analyze the data; HC, XX, JW, TZ, CT and HL provided constructive comments on this study.

CRediT authorship contribution statement

Jun Zhu: Writing – review & editing, Writing – original draft, Visualization, Validation, Software, Methodology, Investigation, Funding acquisition, Data curation. **Xu Yue:** Writing – review & editing, Supervision, Resources, Methodology, Conceptualization. **Hao Zhou:** Software, Methodology, Data curation. **Huizheng Che:** Writing – review & editing, Resources. **Xiangao Xia:** Writing – review & editing, Conceptualization. **Jun Wang:** Writing – review & editing. **Tianliang Zhao:** Writing – review & editing. **Chenguang Tian:** Software. **Hong Liao:** Writing – review & editing.

Declaration of competing interest

The authors declare that they have no known competing financial interests or personal relationships that could have appeared to influence the work reported in this paper.

Data availability

Data will be made available on request.

Acknowledgments

This research was supported by the National Key Research and Development Program of China (2023YFF0805402), National Natural Science Foundation of China (Grant 42030608 and 41975161) and the Jiangsu Science Fund for Carbon Neutrality (Grant BK20220031).

References

- Ajoku, O.F., Miller, A.J., Norris, J.R., 2021. Impacts of aerosols produced by biomass burning on the stratocumulus-to-cumulus transition in the equatorial Atlantic. *Atmospheric Sci. Lett.* 22, e1025 <https://doi.org/10.1002/asl.1025>.
- Akagi, S.K., Yokelson, R.J., Wiedinmyer, C., Alvarado, M.J., Reid, J.S., Karl, T., Crouse, J.D., Wennberg, P.O., 2011. Emission factors for open and domestic biomass burning for use in atmospheric models. *Atmospheric Chem. Phys.* 11, 4039–4072. <https://doi.org/10.5194/acp-11-4039-2011>.
- Ansmann, A., Baars, H., Tesche, M., Müller, D., Althausen, D., Engelmann, R., Pauliquevis, T., Artaxo, P., 2009. Dust and smoke transport from Africa to South America: Lidar profiling over Cape Verde and the Amazon rainforest. *Geophys. Res. Lett.* 36 <https://doi.org/10.1029/2009GL037923>.
- Aouizerats, B., van der Werf, G.R., Balasubramanian, R., Betha, R., 2015. Importance of transboundary transport of biomass burning emissions to regional air quality in Southeast Asia during a high fire event. *Atmospheric Chem. Phys.* 15, 363–373. <https://doi.org/10.5194/acp-15-363-2015>.
- Bey, I., Jacob, D.J., Yantosca, R.M., Logan, J.A., Field, B.D., Fiore, A.M., Li, Q., Liu, H.Y., Mickley, L.J., Schultz, M.G., 2001. Global modeling of tropospheric chemistry with assimilated meteorology: model description and evaluation. *J. Geophys. Res.* Atmospheres 106, 23073–23095. <https://doi.org/10.1029/2001JD000807>.
- Chan, C.Y., Chan, L.Y., Harris, J.M., Oltmans, S.J., Blake, D.R., Qin, Y., Zheng, Y.G., Zheng, X.D., 2003. Characteristics of biomass burning emission sources, transport, and chemical speciation in enhanced springtime tropospheric ozone profile over Hong Kong. *J. Geophys. Res.* Atmospheres 108. <https://doi.org/10.1029/2001JD001555>. ACH 3-1-ACH 3-13.
- Che, H., Xia, X., Zhao, H., Li, L., Gui, K., Zheng, Y., Song, J., Qi, B., Zhu, J., Miao, Y., Wang, Y., Wang, Z., Wang, H., Dubovik, O., Holben, B., Chen, H., Shi, G., Zhang, X., 2024. Aerosol optical and radiative properties and their environmental effects in China: a review. *Earth Sci. Rev.* 248, 104634 <https://doi.org/10.1016/j.earscirev.2023.104634>.
- Chen, J., Li, C., Ristovski, Z., Milic, A., Gu, Y., Islam, M.S., Wang, S., Hao, J., Zhang, H., He, C., Guo, H., Fu, H., Miljevic, B., Morawska, L., Thai, P., Lam, Y.F., Pereira, G., Ding, A., Huang, X., Dumka, U.C., 2017. A review of biomass burning: emissions and impacts on air quality, health and climate in China. *Sci. Total Environ.* 579, 1000–1034. <https://doi.org/10.1016/j.scitotenv.2016.11.025>.
- Choi, J.-O., Chung, C.E., 2014. Sensitivity of aerosol direct radiative forcing to aerosol vertical profile. *Tellus B Chem. Phys. Meteorol.* 66, 24376. <https://doi.org/10.3402/tellusb.v66.24376>.
- Chuvieco, E., Giglio, L., Justice, C., 2008. Global characterization of fire activity: toward defining fire regimes from earth observation data. *Glob. Change Biol.* 14, 1488–1502. <https://doi.org/10.1111/j.1365-2486.2008.01585.x>.
- Dang, R., Liao, H., 2019. Severe winter haze days in the Beijing–Tianjin–Hebei region from 1985 to 2017 and the roles of anthropogenic emissions and meteorology. *Atmospheric Chem. Phys.* 19, 10801–10816. <https://doi.org/10.5194/acp-19-10801-2019>.
- Deng, X., Tie, X., Zhou, X., Wu, D., Zhong, L., Tan, H., Li, F., Huang, X., Bi, X., Deng, T., 2008. Effects of Southeast Asia biomass burning on aerosols and ozone concentrations over the Pearl River Delta (PRD) region. *Atmos. Environ.* 42, 8493–8501. <https://doi.org/10.1016/j.atmosenv.2008.08.013>.
- Ding, A.J., Fu, C.B., Yang, X.Q., Sun, J.N., Petäjä, T., Kerminen, V.-M., Wang, T., Xie, Y., Herrmann, E., Zheng, L.F., Nie, W., Liu, Q., Wei, X.L., Kulmala, M., 2013. Intense atmospheric pollution modifies weather: a case of mixed biomass burning with fossil fuel combustion pollution in eastern China. *Atmospheric Chem. Phys.* 13, 10545–10554. <https://doi.org/10.5194/acp-13-10545-2013>.
- Ding, K., Huang, X., Ding, A., Wang, M., Su, H., Kerminen, V.-M., Petäjä, T., Tan, Z., Wang, Z., Zhou, D., Sun, J., Liao, H., Wang, H., Carslaw, K., Wood, R., Zuidema, P., Rosenfeld, D., Kulmala, M., Fu, C., Pöschl, U., Cheng, Y., Andreae, M.O., 2021. Aerosol-boundary-layer-monsoon interactions amplify semi-direct effect of biomass smoke on low cloud formation in Southeast Asia. *Nat. Commun.* 12, 1–9. <https://doi.org/10.1038/s41467-021-26728-4>.
- Donnelly, J., Daneshkhan, A., Abolfathi, S., 2024. Forecasting global climate drivers using Gaussian processes and convolutional autoencoders. *Eng. Appl. Artif. Intel.* 107536 <https://doi.org/10.1016/j.engappai.2023.107536>.
- Engling, G., Zhang, Y.-N., Chan, C.-Y., Sang, X.-F., Lin, M., Ho, K.-F., Li, Y.-S., Lin, C.-Y., Lee, J.J., 2011. Characterization and sources of aerosol particles over the southeastern Tibetan plateau during the Southeast Asia biomass-burning season. *Tellus B Chem. Phys. Meteorol.* 63, 117–128. <https://doi.org/10.1111/j.1600-0889.2010.00512.x>.
- Fan, W., Li, Jie, Han, Z., Wu, J., Zhang, S., Zhang, C., Li, Jiawei, 2023. Impacts of biomass burning in Southeast Asia on aerosols over the low-latitude plateau in China: an analysis of a typical pollution event. *Front. Environ. Sci.* 11, 1101745 <https://doi.org/10.3389/fenvs.2023.1101745>.
- Ford, B., Val Martin, M., Zelasky, S.E., Fischer, E.V., Anenberg, S.C., Heald, C.L., Pierce, J.R., 2018. Future fire impacts on smoke concentrations, visibility, and health in the contiguous United States. *GeoHealth* 2, 229–247. <https://doi.org/10.1029/2018GH000144>.
- Fox, J., Fujita, Y., Ngidang, D., Peluso, N., Potter, L., Sakuntaladewi, N., Sturgeon, J., Thomas, D., 2009. Policies, political-economy, and Swidden in Southeast Asia. *Hum. Ecol.* 37, 305–322. <https://doi.org/10.1007/s10745-009-9240-7>.
- Giglio, L., Randerson, J.T., van der Werf, G.R., 2013. Analysis of daily, monthly, and annual burned area using the fourth-generation global fire emissions database (GFED4). *J. Geophys. Res. Biogeo.* 118, 317–328. <https://doi.org/10.1002/jgrg.20042>.
- Giorgi, F., Coppola, E., Solmon, F., Mariotti, L., Sylla, M.B., Bi, X., Elguindi, N., Diro, G. T., Nair, V., Giuliani, G., Turuncoglu, U.U., Cozzini, S., Güttler, I., O'Brien, T.A.,

- Tawfik, A.B., Shalaby, A., Zakey, A.S., Steiner, A.L., Stordal, F., Sloan, L.C., Brankovic, C., 2012. RegCM4: model description and preliminary tests over multiple CORDEX domains. *Climate Res.* 52, 7–29. <https://doi.org/10.3354/cr01018>.
- Gong, C., Liao, H., 2019. A typical weather pattern for ozone pollution events in North China. *Atmospheric Chem. Phys.* 19, 13725–13740. <https://doi.org/10.5194/acp-19-13725-2019>.
- Han, X., Zhang, M., Zhu, L., Xu, L., 2013. Model analysis of influences of aerosol mixing state upon its optical properties in East Asia. *Adv. Atmospheric Sci.* 30, 1201–1212. <https://doi.org/10.1007/s00376-012-2150-4>.
- Hantson, S., Arneth, A., Harrison, S.P., Kelley, D.I., Prentice, I.C., Rabin, S.S., Archibald, S., Mouillot, F., Arnold, S.R., Artaxo, P., Bachelet, D., Ciais, P., Forrest, M., Friedlingstein, P., Hickler, T., Kaplan, J.O., Kloster, S., Knorr, W., Lasslop, G., Li, F., Mameon, S., Melton, J.R., Meyn, A., Sitch, S., Spessa, A., van der Werf, G.R., Voulgarakis, A., Yue, C., 2016. The status and challenge of global fire modelling. *Biogeosciences* 13, 3359–3375. <https://doi.org/10.5194/bg-13-3359-2016>.
- Huang, K., Fu, J.S., Hsu, N.C., Gao, Y., Dong, X., Tsay, S.-C., Lam, Y.F., 2013. Impact assessment of biomass burning on air quality in southeast and East Asia during BASE-ASIA. *Atmos. Environ. Observation, modeling and impact studies of biomass burning and pollution in the SE Asian Environment* 78, 291–302. <https://doi.org/10.1016/j.atmosenv.2012.03.048>.
- Huang, X., Ding, A., Liu, L., Liu, Q., Ding, K., Niu, X., Nie, W., Xu, Z., Chi, X., Wang, M., Sun, J., Guo, W., Fu, C., 2016. Effects of aerosol–radiation interaction on precipitation during biomass-burning season in East China. *Atmospheric Chem. Phys.* 16, 10063–10082. <https://doi.org/10.5194/acp-16-10063-2016>.
- Huang, X., Ding, K., Liu, J., Wang, Z., Tang, R., Xue, L., Wang, H., Zhang, Q., Tan, Z.-M., Fu, C., Davis, S.J., Andreae, M.O., Ding, A., 2023. Smoke-weather interaction affects extreme wildfires in diverse coastal regions. *Science* 379, 457–461. <https://doi.org/10.1126/science.add9843>.
- Jian, Y., Fu, T.-M., 2014. Injection heights of springtime biomass-burning plumes over peninsular Southeast Asia and their impacts on long-range pollutant transport. *Atmospheric Chem. Phys.* 14, 3977–3989. <https://doi.org/10.5194/acp-14-3977-2014>.
- Keller, C.A., Long, M.S., Yantosca, R.M., Da Silva, A.M., Pawson, S., Jacob, D.J., 2014. HEMCO v1.0: a versatile, ESMF-compliant component for calculating emissions in atmospheric models. *Geosci. Model Dev.* 7, 1409–1417. <https://doi.org/10.5194/gmd-7-1409-2014>.
- Lei, Y., Yue, X., Liao, H., Gong, C., Zhang, L., 2020. Implementation of Yale interactive terrestrial biosphere model v1.0 into GEOS-Chem v12.0.0: a tool for biosphere–chemistry interactions. *Geosci. Model Dev.* 13, 1137–1153. <https://doi.org/10.5194/gmd-13-1137-2020>.
- Li, J., Zhang, Y., Wang, Z., Sun, Y., Fu, P., Yang, Y., Huang, H., Li, Jianjun, Zhang, Q., Lin, C., Lin, N.-H., 2017b. Regional impact of biomass burning in Southeast Asia on atmospheric aerosols during the 2013 seven south-east Asian studies project. *Aerosol Air Qual. Res.* 17, 2924–2941. <https://doi.org/10.4209/aaqr.2016.09.0422>.
- Li, Jiawei, Han, Z., Surapipith, V., Fan, W., Thongboonchoo, N., Wu, J., Li, Jie, Tao, J., Wu, Y., Macatangay, R., Bran, S.H., Yu, E., Zhang, A., Liang, L., Zhang, R., 2022. Direct and indirect effects and feedbacks of biomass burning aerosols over mainland Southeast Asia and South China in springtime. *Sci. Total Environ.* 842, 156949. <https://doi.org/10.1016/j.scitotenv.2022.156949>.
- Li, M., Zhang, Q., Kurokawa, J., Woo, J.-H., He, K., Lu, Z., Ohara, T., Song, Y., Streets, D. G., Carmichael, G.R., Cheng, Y., Hong, C., Huo, H., Jiang, X., Kang, S., Liu, F., Su, H., Zheng, B., 2017a. MIX: a mosaic Asian anthropogenic emission inventory under the international collaboration framework of the MICS-Asia and HTAP. *Atmospheric Chem. Phys.* 17, 935–963. <https://doi.org/10.5194/acp-17-935-2017>.
- Li, Y., Liu, J., Han, H., Zhao, T., Zhang, X., Zhuang, B., Wang, T., Chen, H., Wu, Y., Li, M., 2019. Collective impacts of biomass burning and synoptic weather on surface PM_{2.5} and CO in Northeast China. *Atmos. Environ.* 213, 64–80. <https://doi.org/10.1016/j.atmosenv.2019.05.062>.
- Li, Z., Lau, W.K.-M., Ramanathan, V., Wu, G., Ding, Y., Manoj, M.G., Liu, J., Qian, Y., Li, J., Zhou, T., Fan, J., Rosenfeld, D., Ming, Y., Wang, Y., Huang, J., Wang, B., Xu, X., Lee, S.-S., Cribb, M., Zhang, F., Yang, X., Zhao, C., Takemura, T., Wang, K., Xia, X., Yin, Y., Zhang, H., Guo, J., Zhai, P.M., Sugimoto, N., Babu, S.S., Brasseur, G. P., 2016. Aerosol and monsoon climate interactions over Asia. *Rev. Geophys.* 54, 866–929. <https://doi.org/10.1002/2015RG000500>.
- Liang, X., Li, S., Zhang, S., Huang, H., Chen, S.X., 2016. PM_{2.5} data reliability, consistency, and air quality assessment in five Chinese cities. *J. Geophys. Res. Atmospheres* 121, 10,220–10,236. <https://doi.org/10.1002/2016JD024877>.
- Lin, C.-Y., Zhao, C., Liu, X., Lin, N.-H., Chen, W.-N., 2014b. Modelling of long-range transport of Southeast Asia biomass-burning aerosols to Taiwan and their radiative forcings over East Asia. *Tellus B Chem. Phys. Meteorol.* 66, 23733. <https://doi.org/10.3402/tellusb.v66.23733>.
- Lin, J.-T., McElroy, M.B., 2010. Impacts of boundary layer mixing on pollutant vertical profiles in the lower troposphere: implications to satellite remote sensing. *Atmos. Environ.* 44, 1726–1739. <https://doi.org/10.1016/j.atmosenv.2010.02.009>.
- Lin, N.-H., Sayer, A.M., Wang, S.-H., Loftus, A.M., Hsiao, T.-C., Sheu, G.-R., Hsu, N.C., Tsay, S.-C., Chantara, S., 2014a. Interactions between biomass-burning aerosols and clouds over Southeast Asia: current status, challenges, and perspectives. *Environ. Pollut.* 195, 292–307. <https://doi.org/10.1016/j.envpol.2014.06.036>.
- Lin, S.-J., Rood, R.B., 1996. Multidimensional flux-form semi-Lagrangian transport schemes. *Mon. Weather Rev.* 124, 2046–2070. [https://doi.org/10.1175/1520-0493\(1996\)124<2046:MFFSLT>2.0.CO;2](https://doi.org/10.1175/1520-0493(1996)124<2046:MFFSLT>2.0.CO;2).
- Liu, H., Jacob, D.J., Bey, I., Yantosca, R.M., 2001. Constraints from 210Pb and 7Be on wet deposition and transport in a global three-dimensional chemical tracer model driven by assimilated meteorological fields. *J. Geophys. Res. Atmospheres* 106, 12109–12128. <https://doi.org/10.1029/2000JD900839>.
- Liu, L., Cheng, Y., Wang, S., Wei, C., Pöhlker, M.L., Pöhlker, C., Artaxo, P., Shrivastava, M., Andreae, M.O., Pöschl, U., Su, H., 2020. Impact of biomass burning aerosols on radiation, clouds, and precipitation over the Amazon: relative importance of aerosol–cloud and aerosol–radiation interactions. *Atmospheric Chem. Phys.* 20, 13283–13301. <https://doi.org/10.5194/acp-20-13283-2020>.
- Mielonen, T., Portin, H., Komppula, M., Leskinen, A., Tamminen, J., Ialongo, I., Hakkarainen, J., Lehtinen, K.E.J., Arola, A., 2012. Biomass burning aerosols observed in eastern Finland during the Russian wildfires in summer 2010 – part 2: remote sensing. *Atmos. Environ.* 47, 279–287. <https://doi.org/10.1016/j.atmosenv.2011.07.016>.
- Mu, M., Randerson, J.T., van der Werf, G.R., Giglio, L., Kasibhatla, P., Morton, D., Collatz, G.J., DeFries, R.S., Hyer, E.J., Prins, E.M., Griffith, D.W.T., Wunch, D., Toon, G.C., Sherlock, V., Wennberg, P.O., 2011. Daily and 3-hourly variability in global fire emissions and consequences for atmospheric model predictions of carbon monoxide. *J. Geophys. Res. Atmospheres* 116. <https://doi.org/10.1029/2011JD016245>.
- Péré, J.C., Bessagnet, B., Mallet, M., Waquet, F., Chiapello, I., Minvielle, F., Pont, V., Menut, L., 2014. Direct radiative effect of the Russian wildfires and its impact on air temperature and atmospheric dynamics during August 2010. *Atmospheric Chem. Phys.* 14, 1999–2013. <https://doi.org/10.5194/acp-14-1999-2014>.
- Pilinis, C., Pandis, Spyros N., Seinfeld, John H., 1995. Sensitivity of direct climate forcing by atmospheric aerosols to aerosol size and composition. *J. Geophys. Res. Atmospheres* 100, 18739–18754. <https://doi.org/10.1029/95JD02119>.
- Ramanathan, V., Ramana, M.V., Roberts, G., Kim, D., Corrigan, C., Chung, C., Winker, D., 2007. Warming trends in Asia amplified by brown cloud solar absorption. *Nature* 448, 575–578. <https://doi.org/10.1038/nature06019>.
- Saide, P.E., Spak, S.N., Pierce, R.B., Otkin, J.A., Schaack, T.K., Heidinger, A.K., da Silva, A.M., Kacenenbogen, M., Redemann, J., Carmichael, G.R., 2015. Central American biomass burning smoke can increase tornado severity in the U.S. *Geophys. Res. Lett.* 42, 956–965. <https://doi.org/10.1002/2014GL028286>.
- Stoerk, T., 2016. Statistical corruption in Beijing’s air quality data has likely ended in 2012. *Atmos. Environ.* 127, 365–371. <https://doi.org/10.1016/j.atmosenv.2015.12.055>.
- Stone, E.A., Lough, G.C., Schauer, J.J., Praveen, P.S., Corrigan, C.E., Ramanathan, V., 2007. Understanding the origin of black carbon in the atmospheric brown cloud over the Indian Ocean. *J. Geophys. Res. Atmospheres* 112. <https://doi.org/10.1029/2006JD008118>.
- Streets, D.G., Yarber, K.F., Woo, J.-H., Carmichael, G.R., 2003. Biomass burning in Asia: annual and seasonal estimates and atmospheric emissions. *Global Biogeochem. Cycles* 17. <https://doi.org/10.1029/2003GB002040>.
- Tian, C., Yue, X., Zhu, J., Liao, H., Yang, Y., Chen, L., Zhou, X., Lei, Y., Zhou, H., Cao, Y., 2023. Projections of fire emissions and the consequent impacts on air quality under 1.5 °C and 2 °C global warming. *Env. Pollut.* 323, 121311. <https://doi.org/10.1016/j.envpol.2023.121311>.
- Tosca, M.G., Randerson, J.T., Zender, C.S., 2013. Global impact of smoke aerosols from landscape fires on climate and the Hadley circulation. *Atmospheric Chem. Phys.* 13, 5227–5241. <https://doi.org/10.5194/acp-13-5227-2013>.
- Tuccella, P., Curci, G., Pitari, G., Lee, S., Jo, D.S., 2020. Direct radiative effect of absorbing aerosols: sensitivity to mixing state, Brown carbon, and soil dust refractive index and shape. *J. Geophys. Res. Atmospheres* 125, e2019JD030967. <https://doi.org/10.1029/2019JD030967>.
- Wang, J., Christopher, S.A., 2006. Mesoscale modeling of central American smoke transport to the United States: 2. Smoke radiative impact on regional surface energy budget and boundary layer evolution. *J. Geophys. Res. Atmospheres* 111. <https://doi.org/10.1029/2005JD006720>.
- van der Werf, G.R., Randerson, J.T., Giglio, L., van Leeuwen, T.T., Chen, Y., Rogers, B.M., Mu, M., van Marle, M.J.E., Morton, D.C., Collatz, G.J., Yokelson, R.J., Kasibhatla, P. S., 2017. Global fire emissions estimates during 1997–2016. *Earth Syst. Sci. Data* 9, 697–720. <https://doi.org/10.5194/essd-9-697-2017>.
- Wesely, M.L., 1989. Parameterization of surface resistances to gaseous dry deposition in regional-scale numerical models. *Atmospheric Environ.* 1967 (23), 1293–1304. [https://doi.org/10.1016/0004-6981\(89\)90153-4](https://doi.org/10.1016/0004-6981(89)90153-4).
- Williams, J.E., Weele, M. van, Velthoven, P.F.J. van, Scheele, M.P., Lioussé, C., van der Werf, G.R., 2012. The impact of uncertainties in African biomass burning emission estimates on modeling global air quality, long range transport and tropospheric chemical lifetimes. *Atmosphere* 3, 132–163. doi:10.3390/atmos3010132.
- Wu, S., Mickle, L.J., Jacob, D.J., Logan, J.A., Yantosca, R.M., Rind, D., 2007. Why are there large differences between models in global budgets of tropospheric ozone? *J. Geophys. Res. Atmospheres* 112. <https://doi.org/10.1029/2006JD007801>.
- Xing, L., Bei, N., Guo, J., Wang, Q., Liu, S., Han, Y., Pongpiachan, S., Li, G., 2021. Impacts of biomass burning in peninsular Southeast Asia on PM_{2.5} concentration and ozone formation in southern China during springtime—a case study. *J. Geophys. Res. Atmospheres* 126, e2021JD034908. <https://doi.org/10.1029/2021JD034908>.
- Xu, R., Tie, X., Li, G., Zhao, S., Cao, J., Feng, T., Long, X., 2018. Effect of biomass burning on black carbon (BC) in South Asia and Tibetan plateau: the analysis of WRF-Chem modeling. *Sci. Total Environ.* 645, 901–912. <https://doi.org/10.1016/j.scitotenv.2018.07.165>.
- Yang, Q., Zhao, T., Tian, Z., Kanike, R., Chang, J., Hu, W., Shu, Z., Hu, J., 2022b. The cross-border transport of PM_{2.5} from the southeast Asian biomass burning emissions and its impact on air pollution in Yunnan plateau, Southwest China. *Remote Sens. (Basel)* 14, 1886. <https://doi.org/10.3390/rs14081886>.
- Yang, S., Lau, W.K.M., Ji, Z., Dong, W., Yang, Song, 2022a. Impacts of radiative effect of pre-monsoon biomass burning aerosols on atmospheric circulation and rainfall over Southeast Asia and southern China. *Climate Dynam.* 59, 417–432. <https://doi.org/10.1007/s00382-021-06135-7>.

- Yeganeh-Bakhtary, A., EyvazOghli, H., Shabakhty, N., Kamranzad, B., Abolfathi, S., 2022. Machine learning as a downscaling approach for prediction of wind characteristics under future climate change scenarios. *Complexity* 2022, e8451812. <https://doi.org/10.1155/2022/8451812>.
- Yin, S., 2020. Biomass burning spatiotemporal variations over south and Southeast Asia. *Environ. Int.* 145, 106153 <https://doi.org/10.1016/j.envint.2020.106153>.
- Yin, S., Wang, X., Zhang, X., Guo, M., Miura, M., Xiao, Y., 2019. Influence of biomass burning on local air pollution in mainland Southeast Asia from 2001 to 2016. *Environ. Pollut.* 254, 112949 <https://doi.org/10.1016/j.envpol.2019.07.117>.
- Yue, X., Liao, H., 2012. Climatic responses to the shortwave and longwave direct radiative effects of sea salt aerosol in present day and the last glacial maximum. *Climate Dynam.* 39, 3019–3040. <https://doi.org/10.1007/s00382-012-1312-5>.
- Yue, X., Unger, N., 2017. Aerosol optical depth thresholds as a tool to assess diffuse radiation fertilization of the land carbon uptake in China. *Atmospheric Chem. Phys.* 17, 1329–1342. <https://doi.org/10.5194/acp-17-1329-2017>.
- Yue, X., Wang, H., Liao, H., Fan, K., 2010. Simulation of dust aerosol radiative feedback using the GMOD: 2. Dust-climate interactions. *J. Geophys. Res. Atmospheres* 115. <https://doi.org/10.1029/2009JD012063>.
- Zhang, A., Wang, Y., Zhang, Y., Weber, R.J., Song, Y., Ke, Z., Zou, Y., 2019. Modeling global radiative effect of brown carbon: A larger heating source in the tropical free troposphere than black carbon. <https://doi.org/10.5194/acp-2019-594>.
- Zhang, L., Gong, S., Padro, J., Barrie, L., 2001. A size-segregated particle dry deposition scheme for an atmospheric aerosol module. *Atmos. Environ.* 35, 549–560. [https://doi.org/10.1016/S1352-2310\(00\)00326-5](https://doi.org/10.1016/S1352-2310(00)00326-5).
- Zhang, L., Ding, S., Qian, W., Zhao, A., Zhao, Shimin, Yang, Y., Weng, G., Tao, M., Chen, H., Zhao, Shaohua, Wang, Z., 2022. The impact of Long-range transport of biomass burning emissions in Southeast Asia on southern China. *Atmosphere* 13. <https://doi.org/10.3390/atmos13071029>.
- Zhang, N., Cao, J., Wang, Q., Huang, R., Zhu, C., Xiao, S., Wang, L., 2018. Biomass burning influences determination based on PM2.5 chemical composition combined with fire counts at southeastern Tibetan plateau during pre-monsoon period. *Atmospheric Res.* 206, 108–116. <https://doi.org/10.1016/j.atmosres.2018.02.018>.
- Zhang, Xutao, Gui, K., Liao, T., Li, Y., Wang, X., Zhang, Xiaoling, Ning, H., Liu, W., Xu, J., 2021. Three-dimensional spatiotemporal evolution of wildfire-induced smoke aerosols: a case study from Liangshan, Southwest China. *Sci. Total Environ.* 762, 144586 <https://doi.org/10.1016/j.scitotenv.2020.144586>.
- Zhao, R., Lee, A.K.Y., Huang, L., Li, X., Yang, F., Abbatt, J.P.D., 2015. Photochemical processing of aqueous atmospheric brown carbon. *Atmospheric Chem. Phys.* 15, 6087–6100. <https://doi.org/10.5194/acp-15-6087-2015>.
- Zhou, H., Yue, X., Lei, Y., Tian, C., Zhu, J., Ma, Y., Cao, Y., Yin, X., Zhang, Z., 2022. Distinguishing the impacts of natural and anthropogenic aerosols on global gross primary productivity through diffuse fertilization effect. *Atmospheric Chem. Phys.* 22, 693–709. <https://doi.org/10.5194/acp-22-693-2022>.
- Zhu, J., Che, H., Xia, X., Chen, H., Goloub, P., Zhang, W., 2014. Column-integrated aerosol optical and physical properties at a regional background atmosphere in North China plain. *Atmos. Environ.* 84, 54–64. <https://doi.org/10.1016/j.atmosenv.2013.11.019>.
- Zhu, J., Xia, X., Che, H., Wang, J., Zhang, J., Duan, Y., 2016. Study of aerosol optical properties at Kunming in Southwest China and long-range transport of biomass burning aerosols from North Burma. *Atmospheric Res.* 169, 237–247. <https://doi.org/10.1016/j.atmosres.2015.10.012>.
- Zhu, J., Yue, X., Che, H., Xia, X., Lei, Y., Wang, J., Zhao, T., Yu, X., Zhou, H., Liao, H., 2022. Contribution of fire emissions to PM2.5 and its transport mechanism over the Yungui plateau, China during 2015–2019. *J. Geophys. Res. Atmospheres* 127, e2022JD036734. <https://doi.org/10.1029/2022JD036734>.